Two-fluid regularised $\mu(I)$-rheology with OpenFOAM

T. Barker & M. Rauter

January 26, 2018

1 Introduction

Here we implement and test a two-fluid formulation designed to capture the evolution of sharp interfaces between granular material and air. The assumption is that both fluids are incompressible and that the air plays little role in the evolution of the flow fields and free-surface of the granular material. A major novelty of this implementation of the equations is that we have coded the constitutive model for granular flow, namely the $\mu(I)$-rheology, in OpenFOAM (Weller, Tabor, Jasak & Fureby, 1998). This allows many existing finite-volume solvers, discretisation schemes and free-surface capturing methods to be readily employed

2 Uniform inclined plane flow

2.1 Problem outline

Two incompressible fluids occupy the square domain $0 < z < L$, $0 < x < L$ with granular material of viscosity η_g and density ρ_* at the bottom $0 < z < h_0$ and Newtonian fluid (η_f, ρ_f) in the region $h_0 < z < L$ above. It is assumed that the volume fraction of the Newtonian phase is unity whereas the granular phase has the constant value $\phi = \phi_0$. The domain is periodic in x and has a no-slip condition along the base located at $z = 0$. At the top of the domain, where $z = L$, the pressure p and normal gradient of the downstream velocity $\partial_z u$ vanish. Flow is driven by gravity such that the geometry represents a semi-infinite frictional plane inclined at an angle ζ.

2.2 Governing equations

We aim to find a steady solution of the momentum balance equations assuming that the flow is uni-directional i.e. $\underline{u} = (u(z), 0, 0)$, $p = p(z)$. As such, the general 2D momentum balance equations consist of an x-component

$$\partial_z \left(\eta \partial_z u\right) + \rho\phi g_x = 0\,, \tag{1}$$

and z-component

$$-\partial_z p + \rho\phi g_z = 0\,, \tag{2}$$

where the gravitational vector $\underline{g} = (g\sin\zeta, -g\cos\zeta)$. At $z = h_0$ we have a discontinuity in viscosity and density. The Newtonian viscosity $\eta = \eta_f$ is constant whereas the granular fluid viscosity (as in Jop, Forterre & Pouliquen, 2006),

$$\eta_g = \frac{\mu(I)p}{\partial_z u}\,, \tag{3}$$

depends on the strain-rate, pressure and the inertial number

$$I = \frac{d\partial_z u}{\sqrt{p/\rho_*}}\,. \tag{4}$$

As an initial test we will use the functional form proposed by Jop, Forterre & Pouliquen (2005) where

$$\mu(I) = \mu_s + \frac{\mu_d - \mu_s}{I_0/I + 1}\,. \tag{5}$$

Here $\mu_s = \tan(\zeta_s)$ and $\mu_d = \tan(\zeta_d)$ are the friction coefficients at the limiting angles for static $\zeta < \zeta_s$ and accelerating $\zeta > \zeta_d$ flow respectively and I_0 is taken to be a material constant.

$\mu_s = 0.383$	$\mu_d = 0.643$	$I_0 = 0.279$
$d = 1 \times 10^{-4}$ m	$\rho_* = 2500$ kg/m^3	$\phi_0 = 0.6$
$\rho_f = 1$ kg/m^3	$\eta_f = 1.48 \times 10^{-5}$ kg/(m·s)	$\zeta = 25^\circ$
$L = 9 \times 10^{-4}$ m	$h_0 = 5 \times 10^{-4}$ m	$g = 9.81$ m/s^2

Table 1: Parameter values used unless specified otherwise.

2.3 Boundary conditions

It is assumed that the granular fluid sits on a rough base such that $u(z = 0) = 0$. At the top of the domain there is a no outflow condition on the Newtonian fluid such that $p(L) = 0$, $\partial_z u(L) = 0$. At the boundary between the two fluids, the fields (u and p) are continuous.

2.4 Exact solution

Starting with the z momentum balance (2), the hydrostatic pressure distribution is obtained

$$p(z) = g\cos\zeta \begin{cases} \rho_*\phi_0(h_0 - z) + \rho_f(L - h_0) & \text{for } z < h_0 \\ \rho_f(L - z) & \text{for } z > h_0 \end{cases} \tag{6}$$

Similarly, from the x momentum balance we have a solution for the deviatoric stresses

$$\eta\partial_z u = \begin{cases} \mu(I)p(z) \\ \eta_f\partial_z u \end{cases} = -g\sin\zeta \begin{cases} \rho_*\phi_0 z + c_1 & \text{for } z < h_0 \\ \rho_f z + c_2 & \text{for } z > h_0 \end{cases} \tag{7}$$

applying the neumann condition at $z = L$ and enforcing continuity at $z = h$ gives the integration constants as $c_1 = \rho_f(h_0 - L) - \rho_*\phi_0 h_0$ and $c_2 = -\rho_f L$. As such, we have

$$\mu(I) = \tan\zeta\,, \tag{8}$$

in the granular phase which implies that the inertial number is a constant i.e. $I = I_\zeta = \mu^{-1}(\tan\zeta)$. This means that (4) can be solved to give the Bagnold velocity field in the granular flow and (7) can be solved for the Newtonian fluid to give the Poiseuille velocity solution such that

$$u(z) = \begin{cases} \dfrac{-2I_\zeta\sqrt{g\cos\zeta}}{3d\rho_*^{3/2}\phi_0}\left[\rho_*\phi_0(h_0 - z) + \rho_f(L - h_0)\right]^{3/2} + c_3 & \text{for } z < h_0 \\ \dfrac{\rho_f g\sin\zeta}{\eta_f}\left(Lz - \dfrac{z^2}{2} + c_4\right) & \text{for } z > h_0 \end{cases} \tag{9}$$

where the constant

$$c_3 = -\frac{2I_\zeta\sqrt{g\cos\zeta}}{3d\rho_*^{3/2}\phi_0}\left[\rho_*\phi_0 h_0 + \rho_f(h_0 - L)\right]^{3/2}\,, \tag{10}$$

is found by applying the no-slip condition and

$$c_4 = \frac{2\eta_f I_\zeta\sqrt{\cos\zeta}}{3d\sqrt{g}\rho_*^{3/2}\phi_0\sin\zeta}(h_0 - L)^{3/2} - Lh_0 + \frac{h_0^2}{2} + \frac{\eta_f c_3}{\rho_f g\sin\zeta}\,, \tag{11}$$

is due to the matching at $z = h_0$.

3 Numerical validation

Here we employ OpenFOAM to solve the full 2D transient equations to validate the exact steady solution and the discretised implementation. We modify the solver 'interFoam' that uses the Volume Of Fluid (VOF) method to capture the evolution of the interface between the two fluids. This approach is very similar to that used in the Gerris code (Popinet, 2003) that is often used for granular flow simulations.

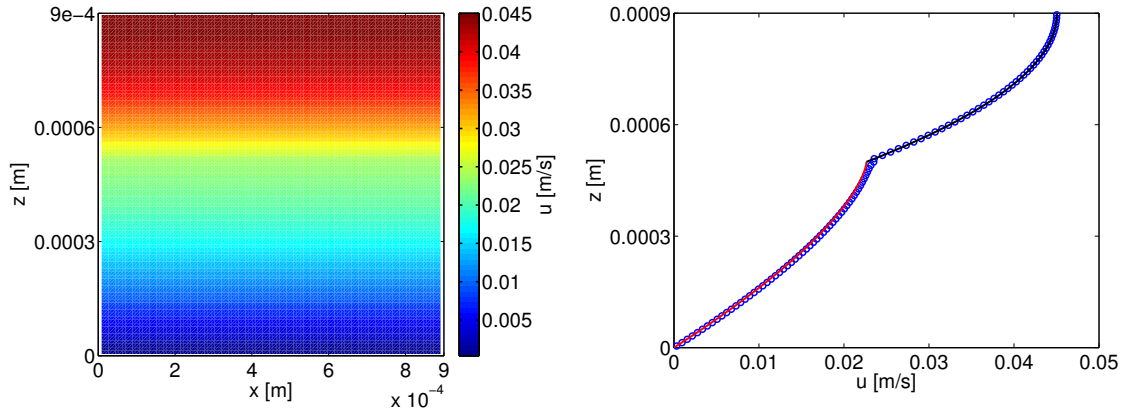

Figure 1: The downstream velocity u at $t = 10$ s evaluated at the cell centres (left) and averaged along the x direction (right). In the right figure, the solid red line is the Bagnold velocity profile while the solid black line is the matching Poiseuille flow in the Newtonian fluid above. The granular media occupies $0 < z < h_0$ where $h_0 = 5 \times 10^{-4}$ m and the computational domain is square. Each coordinate spans nine grain diameters and is discretised with 50×100 computational cells.

A scalar tracer T defines the volume of each constituent with $T = 0$ being pure Newtonian fluid and $T = 1$ being pure granular. This tracer is advected with the flow via the equation

$$\partial_t T + \nabla \cdot (T\underline{u}) = 0\,. \tag{12}$$

Material properties at a location are then defined in terms of T with, for example, the density being

$$\rho = T\rho_* \phi_0 + (1 - T)\rho_f\,, \tag{13}$$

and the dynamic viscosity

$$\eta = \frac{T\rho_* \phi_0 \eta_g + (1 - T)\rho_f \eta_f}{T\rho_* \phi_0 + (1 - T)\rho_f}\,. \tag{14}$$

Interestingly, and perhaps importantly, often in Gerris (e.g. Lagrée, Staron & Popinet, 2011) the viscosity is defined as

$$\eta = \frac{1}{\dfrac{T}{\eta_g} + \dfrac{1 - T}{\eta_f}}\,, \tag{15}$$

i.e. the harmonic mean of the viscosities and without weighting with density. Being a discretised solution of the advection equation, boundaries between the two phases are slightly diffuse rather than being a discontinuous shock. However, finer meshes will reduce the thickness of this diffuse matching layer and tend towards the exact steady solution for long times, as shown in figure 1.

3.1 Well-posed vs. ill-posed behaviour

As detailed in Barker, Schaeffer, Bohorquez & Gray (2015) the $\mu(I)$-rheology of Jop *et al.* (2006) is ill-posed for large inclination angles $\zeta \gtrsim 30^\circ$ and for low angles $\zeta \lesssim 22^\circ$. For the parameters listed in table 1, the maximum angle for steady flow is $\zeta_d \approx 32.7^\circ$ so a simulation at $\zeta = 32^\circ$ should be unstable due to ill-posedness despite the steady solution derived in §2 being well defined. Here we verify that the implementation outlined here similarly does not converge on the steady uniform solution. The numerical scheme is very different from Gerris and so we don't expect identical results. However the disparity in the viscosity weighting, as highlighted in the difference between (14) and (15), can be readily checked to ensure that the ill-posedness is present regardless of this aspect of the implementation. As shown in figure 2, the two variants have qualitatively similar features but differ quite drastically in the precise values of the pressure perturbations. In both cases the pressure in the granular material has become negative so that the solver automatically regularises the value of the inertial number and viscosity. As

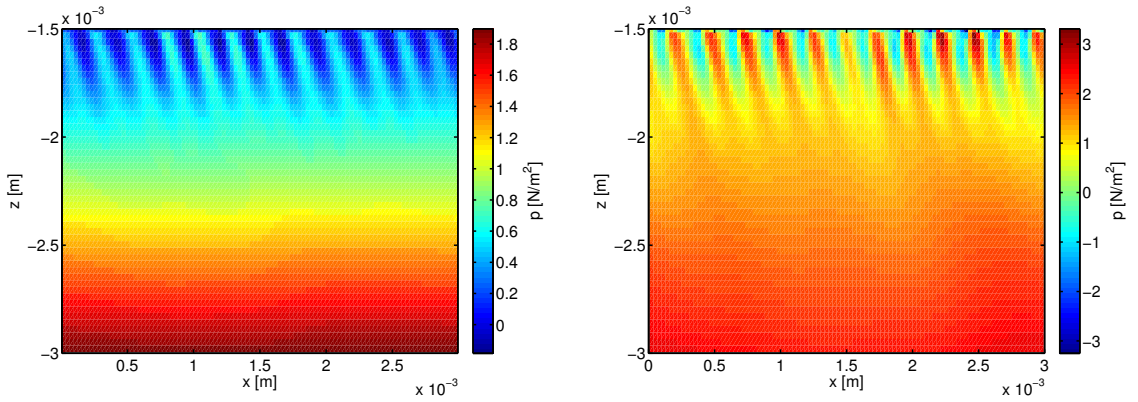

Figure 2: The pressure p in the granular material at $t = 0.04$ s at the ill-posed angle of 32°. Left is with the standard OpenFOAM viscosity definition (14) and right is with the harmonic mean definition used by Gerris (15).

$$\mu_s = 0.342 \qquad \mu_d = 0.557 \qquad I_0 = 0.069 \qquad d = 1.43 \times 10^{-4}\ \text{m}$$

Table 2: Parameter values used in §3.2 for comparison with Barker & Gray (2017).

such, neither result represents a reliable prediction of the transient pressure field in a real flow and all the qualitative features can be safely attributed to the ill-posedness of the rheology at this inclination angle.

3.2 Regularisation by changing the $\mu(I)$ curve

As demonstrated by Barker & Gray (2017), the incompressible equations for granular flow suggested by Jop *et al.* (2006) may be regularised for all inertial numbers, below some large maximal value, through modification of the functional form of the $\mu(I)$ relation. This allows for stable calculations with I in the previously ill-posed ranges $I < I_1^N$ and $I > I_2^N$. The chosen form is

$$\mu(I) = \begin{cases} \sqrt{\dfrac{\alpha}{\ln(\frac{A_-}{I})}} & I \leq I_1^N \\ \dfrac{\mu_s I_0 + \mu_d I + \mu_\infty I^2}{I_0 + I} & I > I_1^N \end{cases}, \tag{16}$$

where the lower inertial number branch is derived from the condition for well-posedness and the curve for large inertial numbers is inspired by experimental data. In (16) there are additional material parameters μ_∞ and α, compared to the functional form in (5), whereas

$$A_- = I_1^N \exp\left(\frac{\alpha(I_0 + I_1^N)^2}{(\mu_s I_0 + \mu_d I_1^N + \mu_\infty (I_1^N)^2)^2}\right), \tag{17}$$

is defined explicitly. Well-posed behaviour is found for small inertial numbers with $\alpha \lesssim 2$ and for large inertial numbers experimental measurements of steady chute flow are well fitted with $\mu_\infty = 0.05$. Figure 3 shows the results of calculations that are identical apart from the $\mu(I)$ curve used. Here we can see that without the regularisation, perturbations form spontaneously for flows at large inclination angles but do not form when the regularised curve is (16) is used.

4 Complex free-surface evolution

Combining the two-phase incompressible solver with the regularised $\mu(I)$-rheology for the granular phase, one should be able to simulate the flow of granular materials in more complicated scenarios that the

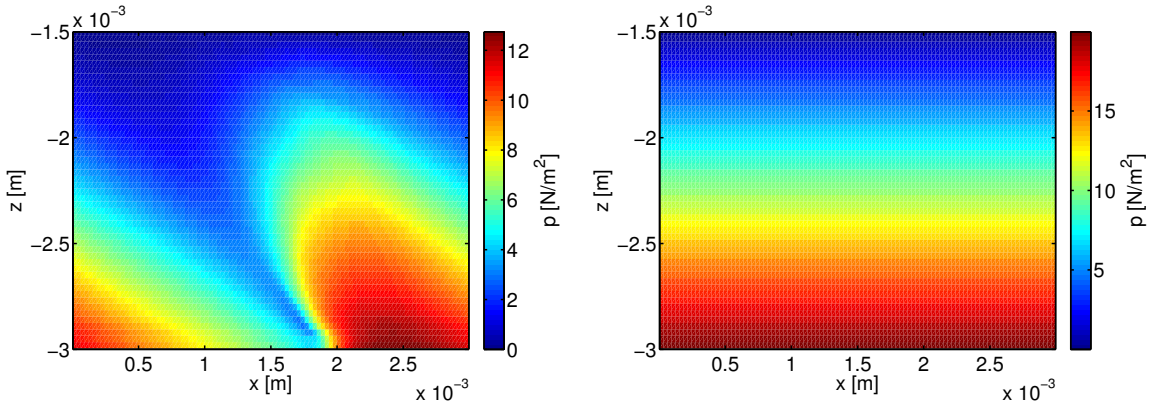

Figure 3: The pressure in simulations of two-fluid chute flow at $\zeta = 28.5^\circ$ with parameters from table 2. Left is at $t = 0.2$ s using the Jop *et al.* (2006) $\mu(I)$ curve, which is ill-posed at this angle, whereas the right is at $t = 2$ s using the regularised form (16), which is well-posed.

periodic, uniform situation tested thus far. In the past similar methods have been used to simulate column collapses (Lagrée *et al.*, 2011), silo flows (Staron, Lagrée & Popinet, 2012) and granular rollwaves (Barker & Gray, 2017). Here we would like to look at other problems which probe the validity of the $\mu(I)$-rheology and our numerical implementation. Of great interest is the transition from and to static material. In the regularised rheology (16) static material corresponds to $I = 0$ and therefore a vanishing granular viscosity as $\mu(0) = 0$. It is not yet known how static material evolves away from this point, just that decelerating flows have a roughly exponential decay in I leading to slower and slower creeping velocities (see Barker & Gray, 2017). We would like to consider again the column collapse problem, as this initially has $I = 0$ everywhere. To further validate the applicability of our numerical solver, we will do the column collapse on a finite inclined plane that leads to a flat run-out area via a curved transition.

Another problem of interest, where grain interchange between static and moving areas, is in moving shocks. When a granular avalanche on a inclined plane hits an impenetrable vertical wall, a shock will form that will move back up the slope. Downslope of the shock front one expects material to approach a static state as the pressure will increase as material builds up. It is also of interest to compare the stage before impact to the wall as two-dimensional simulations of a granular flow front have not yet been performed. The shape of this front can be directly compared to the solution of the depth-averaged $\mu(I)$ equations of Gray & Edwards (2014) using the derivation originally supplied by Pouliquen (1999).

4.1 Mass release on a slope with a flat run-out area

4.2 Granular flow front

4.3 Uphill travelling shock

References

Barker, T. & Gray, J. 2017 Partial regularisation of the incompressible $\mu(I)$-rheology for granular flow. *Journal of Fluid Mechanics* **828**, 5–32.

Barker, T., Schaeffer, D. G., Bohorquez, P. & Gray, J. M. N. T. 2015 Well-posed and ill-posed behaviour of the $\mu(I)$-rheology for granular flow. *J. Fluid Mech.* **779**, 794–818.

Gray, J. M. N. T. & Edwards, A. N. 2014 A depth-averaged $\mu(I)$-rheology for shallow granular free-surface flows. *J. Fluid Mech.* **755**, 503–534.

Jop, P., Forterre, Y. & Pouliquen, O. 2005 Crucial role of sidewalls in granular surface flows: consequences for the rheology. *J. Fluid Mech.* **541**, 167.

Jop, P., Forterre, Y. & Pouliquen, O. 2006 A constitutive relation for dense granular flows. *Nature* **44**, 727–730.

Lagrée, P.-Y., Staron, L. & Popinet, S. 2011 The granular column collapse as a continuum: validity of a two-dimensional Navier–Stokes model with a $\mu(I)$-rheology. *J. Fluid Mech.* **686**, 378–408.

Popinet, S. 2003 Gerris: a tree-based adaptive solver for the incompressible euler equations in complex geometries. *J. Comp. Phys.* **190** (2), 572–600.

Pouliquen, O. 1999 On the shape of granular fronts down rough inclined planes. *Physics of Fluids* **11** (7), 1956–1958.

Staron, L., Lagrée, P.-Y. & Popinet, S. 2012 The granular silo as a continuum plastic flow: The hour-glass vs the clepsydra. *Phys. Fluids* **24**, 103301.

Weller, H. G., Tabor, G., Jasak, H. & Fureby, C. 1998 A tensorial approach to computational continuum mechanics using object-oriented techniques. *Comp. in Phys.* **12** (6), 620–631.